Published in final edited form as:
Neuron. 2009 May 14; 62(3): 375–387. doi:10.1016/j.neuron.2009.04.006.

Harmonin mutations cause mechanotransduction defects in cochlear hair cells

Nicolas Grillet[1,+], **Wei Xiong**[1,+], **Anna Reynolds**[1,+], **Piotr Kazmierczak**[1], **Takashi Sato**[2], **Concepcion Lillo**[3], **Rachel A. Dumont**[4], **Edith Hintermann**[1], **Anna Sczaniecka**[1], **Martin Schwander**[1], **David Williams**[3], **Bechara Kachar**[2], **Peter G. Gillespie**[4], and **Ulrich Müller**[1]

1 *Department of Cell Biology, Institute for Childhood and Neglected Disease, The Scripps Research Institute, 10550 N. Torrey Pines Road, La Jolla, California 92037, USA*

2 *Laboratory of Cellular Biology, National Institute of Deafness and other Communication Disorders, National Institute of Health, Bethesda, Maryland 20892, USA*

3 *Jules Stein Eye Institute, Departments of Ophthalmology and Neurobiology, UCLA School of Medicine, Los Angeles, California*

4 *Oregon Hearing Research Center & Vollum Institute, Oregon Health & Science University, Portland, Oregon 97239, USA*

Abstract

In hair cells, mechanotransduction channels are gated by tip links, the extracellular filaments that consist of cadherin 23 (CDH23) and protocadherin 15 (PCDH15) and connect the stereocilia of each hair cell. However, which molecules mediate cadherin function at tip links is not known. Here we show that the PDZ-domain protein harmonin is a component of the upper tip-link density (UTLD), where CDH23 inserts into the stereociliary membrane. Harmonin domains that mediate interactions with CDH23 and F-actin control harmonin localization in stereocilia and are necessary for normal hearing. In mice expressing a mutant harmonin protein that prevents UTLD formation, the sensitivity of hair bundles to mechanical stimulation is reduced. We conclude that harmonin is a UTLD component and contributes to establishing the sensitivity of mechanotransduction channels to displacement.

Keywords

harmonin; Usher Syndrome; mechanotransduction; stereocilia; hair cells

Introduction

Hair cells of the inner ear are the specialized mechanosensory cells that convert mechanical stimuli arising from sound waves and head movement into electrical signals to provide our senses of hearing and balance. Each hair cell contains at its apical surface F-actin rich stereocilia, which are organized in rows of increasing heights. Mechanotransduction channels

6Corresponding author: The Scripps Research Institute, 10550 North Torrey Pines Road, La Jolla, Ca 92073, Phone: 858-784-7288, Email: E-mail: umueller@scripps.edu.
[+]These authors have contributed equally to the work

are localized close to the tips of the stereocilia (Muller, 2008; Vollrath et al., 2007) and are thought to be gated by an elastic element, the gating spring, which is stretched by excitatory stimuli mediating rapid channel opening (Corey and Hudspeth, 1983). Tip links, which project from the top of a stereocilium and connect to its taller neighbor, parallel to the axis of mechanical sensitivity of the stereociliary bundle, have been proposed to be the gating spring or to be connected to it in series (Pickles et al., 1984). In support of this hypothesis, when tip links are severed, mechanotransduction ceases and the hair bundle moves by more than 100 nm (Assad et al., 1991).

Recent studies have demonstrated that tip links are adhesion complexes formed by PCDH15 and CDH23, which are members of the cadherin superfamily. Mutations in the genes encoding PCDH15 and CDH23 lead to Usher Syndrome, the leading cause of deaf-blindness in humans, and to recessive forms of deafness (Ahmed et al., 2001; Ahmed et al., 2002; Alagramam et al., 2001b; Bolz et al., 2001; Bork et al., 2001; Di Palma et al., 2001). PCDH15 and CDH23 are expressed in developing hair bundles, where they are components of transient lateral links and kinociliary links that are required for hair bundle morphogenesis (Alagramam et al., 2001a; Di Palma et al., 2001; Kazmierczak et al., 2007; Lagziel et al., 2005; Michel et al., 2005; Rzadzinska et al., 2005; Senften et al., 2006; Siemens et al., 2004; Wada et al., 2001; Wilson et al., 2001). In functionally mature hair cells, PCDH15 and CDH23 interact to form tip links, where each tip link is an asymmetric protein complex containing PCDH15 at the lower part and CDH23 at the upper part (Fig. 1a) (Kazmierczak et al., 2007). The two ends of each tip link are anchored at the stereociliary membrane in electron-dense plaques, the upper tip-link density (UTLD) and lower tip-link density (LTLD) (Fig. 1A) (Furness and Hackney, 1985). Tip-link densities are appropriately localized to contain additional components of the mechanotransduction machinery including the transduction channel and molecules that link the channel to the cytoskeleton.

So far, few proteins have been localized to LTLDs (Belyantseva et al., 2005; Delprat et al., 2005), and we do not know the molecular composition of UTLDs. Candidate components of tip-link densities are proteins that interact with the cytoplasmic domains of CDH23 and PCDH15, including the molecular scaffolding protein harmonin. Mutations in harmonin are linked to Usher Syndrome and recessive forms of deafness in humans, mirroring the disease phenotypes caused by mutations in *PCDH15* and *CDH23* (Ahmed et al., 2002; Ouyang et al., 2002; Verpy et al., 2000). Harmonin is expressed as several splice variants, which have been termed harmonin-a, -b, and -c (Fig. 1B) (Verpy et al., 2000). The longest harmonin-b variant, which contains 3 PDZ domains, 2 coiled-coil domains and a domain rich in proline, serine and threonine (PST), is expressed in hair bundles of developing cochlear hair cells (Fig. 1B) (Boeda et al., 2002; Verpy et al., 2000). Harmonin-b binds in vitro to CDH23, PCDH15, F-actin, and to harmonin itself (Adato et al., 2005; Boeda et al., 2002; Kazmierczak et al., 2007; Reiners et al., 2006; Siemens et al., 2002). Harmonin-deficient mice have similar defects in hair bundle morphogenesis as mice with mutations in the CDH23 and PCDH15 genes (Johnson et al., 2003; Lefevre et al., 2008). Collectively, these findings suggest that harmonin is required for cadherin function in hair cell development. A recent publication mentions that harmonin is expressed in hair cells of adult mice (Lefevre et al., 2008), suggesting that harmonin may have additional functions in hair cells that go beyond its developmental role.

To test whether harmonin might have a role in mechanotransduction, we have determined its subcellular localization in functionally mature hair cells and have characterized mechanotransduction currents in a mouse line carrying a mutation in the harmonin gene. We show here that harmonin is concentrated at UTLDs where CDH23 molecules insert into the stereociliary membrane. Harmonin localization is perturbed in mice carrying a missense mutation in the PDZ2 domain of harmonin, which disrupts interactions with CDH23, as well as in mice expressing a harmonin protein lacking the coiled-coil and PST domains, which are

required for binding to F-actin. While the missense mutation in PDZ2 affects hair bundle development, deletion of the coiled-coil and PST domains leaves hair bundle development intact and instead prevents the formation of UTLDs, but not of the tip links. However, the function of the mechanotransduction machinery in hair bundles of cochlear hair is significantly altered in mice expressing the harmonin protein lacking the coiled-coil and PST domains. Interestingly, the properties of transducer currents in the mutant mice share similarities with those in immature cochlear hair cells (Waguespack et al., 2007), suggesting that harmonin is required for the developmental maturation of a hair cell's mechanotransduction machinery.

Results

Harmonin is localized at the UTLDs of functionally mature hair cells

To determine the subcellular distribution of harmonin in hair cells, we raised an antibody (H3) against the PDZ3 domain of harmonin, which is present in harmonin-a and -b splice variants, but not in harmonin-c (Fig. 1B). Affinity-purified H3 antibody recognized harmonin expressed in tissue culture cells (Supplementary Fig. 1A–C). In agreement with earlier studies using similar antibodies (Boeda et al., 2002;Lefevre et al., 2008), H3 detected harmonin in stereocilia of developing hair cells (Fig. 1C), with fluorescence signals visible as single puncta below the tip of each stereocilium (Figs. 1D,2E;Supplementary Fig. 1D). This finding was confirmed by immunoelectron microscopy; gold particles were detected below the tips of stereocilia close to the region where upper tip-link densities (UTLDs) are localized (Fig. 1E,F). To further confirm the specificity of our antibody, we stained cochlear hair cells from *dfcr2J* mice, which carry a mutation truncating the harmonin protein prior to the PDZ3 (Johnson et al., 2003). As expected, H3 did not stain *dfcr2J* stereocilia (Supplementary Fig. 1D).

To determine whether harmonin is a genuine component of UTLDs and present in functionally mature hair cells, we analyzed its localization by immunogold labeling in outer hair cells (OHCs) of P35 animals. Harmonin was prominently localized at UTLDs, but only sparsely at LTLDs (Fig. 1G–J, G′–J′). We quantified the distribution of gold particles in 16 stereocilia pairs where the plane of sectioning revealed tip-link densities. Most (69%) gold particles were localized at UTLDs; the other particles were distributed over the much larger remaining surface area of the stereocilia. Few gold particles were detected at LTLDs (Fig. 1K,L). We conclude that harmonin is expressed in functionally mature hair cells where it is concentrated at UTLDs.

A missense mutation in PDZ2 affects harmonin localization in hair cells as well as hair bundle morphogenesis

The presence of harmonin at UTLDs is reminiscent of the asymmetric distribution of CDH23, which is localized at the upper end of tip links (Fig. 1A) (Kazmierczak et al., 2007). To determine whether the PDZ2 domain of harmonin, which binds in vitro to CDH23 (Boeda et al., 2002;Siemens et al., 2002), is required for harmonin localization in hair cells, we generated mice expressing harmonin incapable of binding to CDH23. Because the PDZ2 domain of harmonin contains a glycine-leucine-glycine (GLG) motif, which in other PDZ domains is critical for mediating interactions with target proteins (Sheng and Sala, 2001), we reasoned that mutation of this motif would disrupt harmonin-CDH23 interactions. We therefore engineered a eukaryotic expression vector containing harmonin PDZ2, substituting the GLG motif with an alanine-alanine-alanine (AAA) motif (Fig. 2A). We next co-expressed in HEK cells wild-type and mutant PDZ2 domains, along with a protein containing the cytoplasmic domain of CDH23 fused to the transmembrane and extracellular domains of the IL2 receptor (IL2-CDH23). Protein complexes were isolated by immunoprecipitation with IL2 antibodies and analyzed by Western blot. While wild-type PDZ2 bound IL2-CDH23, the PDZ2 AAA mutation effectively disrupted this interaction (Fig. 2B). We conclude that the GLG motif in PDZ2 is critical for binding of harmonin to CDH23.

Next, we generated by a knock-in strategy a genetically modified mouse line expressing a harmonin allele carrying the AAA mutation in PDZ2, *harmonin-PDZ2^{AAA}* (Fig. 2A, and Supplementary Fig. 2) (Boeda et al., 2002;Siemens et al., 2002). Homozygous *harmonin-PDZ2$^{AAA/AAA}$* mice were viable but displayed from P10 onwards head tossing and circling behavior indicative of vestibular dysfunction (data not shown). Measurements of the auditory brain stem response (ABR) in 4-week old animals revealed that the mice were profoundly deaf (Fig. 2C, D); wild-type mice had auditory thresholds of ~ 30 dB, while thresholds in the mutants were >90 dB. In addition, hair bundle development was disrupted in *harmonin-PDZ2$^{AAA/AAA}$* mice (Fig. 2E). Harmonin was no longer concentrated below the tips of stereocilia and was instead diffusely distributed in hair bundles (Fig. 2E), demonstrating that the PDZ2 mutation affects harmonin targeting to emerging UTLDs. The striking co-localization of harmonin and CDH23 at the upper part of tip links in wild-type mice, as well as similar defects in hair bundle morphogenesis in *harmonin-PDZ2$^{AAA/AAA}$* mice and *Cdh23*-deficient *waltzer* mice (Di Palma et al., 2001), suggests that harmonin and CDH23 act in hair cells in a common pathway. However, PCDH15 also interacts with the PDZ2 domain of harmonin (Adato et al., 2005;Reiners et al., 2006;Senften et al., 2006), and defects in this interaction might contribute to *harmonin-PDZ2$^{AAA/AAA}$* bundle defects.

Deletion of the coiled-coil and PST domains affects harmonin localization in hair cells but not hair bundle morphogenesis

As the mechanotransduction machinery of hair cells is thought to be linked to the F-actin cytoskeleton, we wondered whether the F-actin binding domain of harmonin might link CDH23 at UTLDs to the cytoskeleton. To test this hypothesis, we examined homozygous *deaf circler* (*dfcr*) mice (Johnson et al., 2003); these mice carry an in-frame deletion in the harmonin gene that removes the coiled-coil and PST domains, which mediate in vitro interactions with F-actin (Fig. 3A) (Boeda et al., 2002). To confirm that the *dfcr* mutation disrupts interactions with F-actin, we expressed in HeLa cells N-terminal GFP fusions of wild-type harmonin-b or the harmonin-*dfcr* variant. In transfected cells, wild-type harmonin-b associates with and bundles F-actin (Boeda et al., 2002). Similarly, GFP-tagged harmonin-b proteins also generated F-actin bundles in transfected HeLa cells (Fig. 3B). These bundles were thicker and more pronounced than in untransfected cells (Fig. 3B, compare upper and middle panels), indicating that GFP-harmonin-b effectively bound to and bundled F-actin. In contrast, GFP-harmonin-*dfcr* remained diffuse within the cytoplasm and did not bundle F-actin (Fig. 3B, upper panels). We also generated a GFP fusion protein of harmonin-b lacking the PDZ2 domain, which was mutated in *harmonin-PDZ2$^{AAA/AAA}$* mice (Fig. 3A). The PDZ2 mutant construct efficiently bound to and bundled F-actin, indicating that PDZ2 is not required for interactions of harmonin-b with F-actin (Fig. 3B, lower panels).

We next analyzed hair bundle morphology in *dfcr* mice. While a previous study revealed defects in the morphology of hair bundles in *dfcr* mice (Johnson et al., 2003), we rarely observed such defects at any position along the cochlear duct in our *dfcr* colony, at least within the first few months after birth (Fig. 3C; Supplementary Fig. 3). However, degenerative changes in the organ of Corti were evident at subsequent ages and also affected spiral ganglion neurons (data not shown). Unlike the previous study, we analyzed the *dfcr* allele on a C57Bl/6J background, suggesting that a genetic modifier locus is responsible for the phenotypic difference. Despite the absence in hair bundle defects, ABR recordings demonstrated that homozygous *dfcr* mice were deaf, by 4 weeks of age, with auditory thresholds >90 dB (Fig. 3D,E).

Importantly, harmonin immunoreactivity in inner hair cells (IHCs) and OHCs of homozygous *dfcr* mice was shifted to the very tips of stereocilia (Fig. 3C; Supplementary Fig. 4). However, the expression of other hair cell proteins such as myosin-1c (MYO1C) appeared unaffected (Supplementary Fig. 4). Taken together, these findings suggest that the coiled-coil and PST

domains of harmonin are required for harmonin localization to UTLDs and for normal hearing, but not for hair bundle development. While deletion of the coiled-coil and PST domains affect F-actin binding, F-actin is distributed too broadly in stereocilia to account alone for the localization of the harmonin at UTLDs, suggesting that the *dfcr* mutation might also affect interactions with other yet to be identified proteins.

UTLDs are absent in homozygous *dfcr* mice

Since the coiled-coil and PST domains of harmonin-b are not essential for hair bundle development, we wondered whether they might have essential functions at UTDLs. Using transmission electron microscopy, we examined UTLDs in homozygous *dfcr* mice at P10, when UTLDs can first be easily detected, and at P18 and P70, when UTLDs have assumed their characteristic cup-shaped appearance (Supplementary Fig. 5). At P10, stereociliary tips in wild-type and homozygous *dfcr* mice showed the typical beveling of the actin core thought to arise from tension exerted by tip links (Fig. 4A–D) (Manor and Kachar, 2008). Tip links were difficult to visualize with our staining conditions but were occasionally observed, even in homozygous *dfcr* mice, suggesting that their formation was not altered by the harmonin mutation (Fig. 4A–D). This interpretation was further supported by the analysis of hair cells using scanning electron microscopy, which revealed appropriately positioned extracellular filaments running from the tip of the shorter stereocilium to the side of its next longer neighbor (Fig. 4O–R), and by our electrophysiological evidence, which demonstrated that mechanotransduction currents could still be evoked in hair cells from *dfcr* mice (see below).

We next evaluated the presence of tip-link densities in serial sections through more than 90 hair bundles each from cochlear hair cells of homozygous *dfcr* mice and wild-type littermates that were processed in parallel. LTLDs were consistently observed both in wild-type and mutant animals; by contrast, UTLDs were also detectable at P10 and P18 in wild-type mice, but not in mutants (Fig. 4A–L). Similar observations were made at P70 (Fig. 4M,N). We conclude that harmonin is a component of UTLDs, and that the mutation in the coiled-coil and PST domains of harmonin affects the formation or stability of UTLDs. Nevertheless, tip links were still present in *dfcr* mice, indicating that tip links form independently of UTLDs.

Defects in mechanotransduction in *dfcr* mice

Harmonin mutations might affect the properties of the mechanotransduction machinery of cochlear hair cells. Because hair bundle morphology was not noticeably affected in *dfcr* mice, their hair cells were ideally suited to test this hypothesis. We measured transducer currents in P7–P8 OHCs from the apical-to-middle part of the cochlea using whole cell recordings, and stimulating with a stiff glass probe. In agreement with previous findings (Kennedy et al., 2003; Kros et al., 2002; Stauffer et al., 2005; Waguespack et al., 2007), control OHCs had rapidly activating transducer currents, which subsequently adapted (Fig. 5A, blue traces); similar current traces were obtained with OHCs from *dfcr* mice (Fig. 5A, red traces). The amplitudes of saturated mechanotransduction currents at maximal deflection (>1 μm) were similar in controls (510 ± 27 pA; mean ± SEM; n=34) and mutants (463 ± 24 pA; mean ± SEM; n=32) (Fig. 5B), suggesting that the total number of transducer channels was not significantly altered in *dfcr* OHCs. To normalize for variations due to cell-to-cell differences in amplitude, we plotted the open probability of the transduction channel (Po) against displacement, and observed that the resulting curve from mutants was significantly shifted to the right and broadened when compared to the wild-type curve (Fig. 5C). The resting potential was comparable in OHCs from wild-type and mutant animals (approximately −50 mV), suggesting that the change in the displacement-Po relationship was not a simple consequence of hair cell deterioration.

Adaptation of transducer currents in hair cells progresses with fast and slow time constants (Gillespie and Cyr, 2004; Kennedy et al., 2003; Waguespack et al., 2007). As a result of adaptation, channels Po resets towards its resting value, which is near the point of optimal sensitivity along the displacement-Po relationship. We reasoned that the rightward shift and broadening of the displacement-Po relationship in *dfcr* mice might result from altered properties of adaptation. We therefore directly determined effects of the mutation on resting Po as well as on adaptation time constants. In wild-type mice, resting Po was 3.4 ± 0.6 % (n=10), but it was significantly reduced in the mutants to 1.3 ± 0.3 % (n=14) (Fig. 5D). To determine whether adaptation was affected, we averaged transducer current traces from each cell in control and mutant animals; we fitted the traces with double exponential functions and determined fast and slow adaptation time constants. Representative current traces for deflection of 200 nm and 400 nm are shown in Fig. 6A. To normalize for the difference in the set point of the displacement-Po relationship, we also compared the data based on Po (Fig. 6B). When we plotted adaptation time constants against Po, we observed that both fast and slow adaptation were significantly slowed in the mutants. The mean τ_{fast} in hair cells from wild-type mice ranged from 0.27 ± 0.04 to 0.33 ± 0.04 ms, depending on the size of the stimulus. By contrast, τ_{fast} was nearly doubled in mutants to a range of 0.46 ± 0.05 ms to 0.54 ± 0.03 ms (mean ± SEM) (Fig. 6C). τ_{slow} in wild-type was between 1.4 ± 0.4 and 2.6 ± 0.5 ms, and in mutants between 2.6 ± 0.3 and 3.5 ± 0.6; mean ± SEM) (Fig. 6C).

The plots in Fig. 6B also indicated that activation of transducer currents at similar Po was significantly slowed in *dfcr* mice. Transduction currents develop with a sigmoidal onset that can be fitted with two time constants; the fast process may be limited by speed of the stimulation and recording systems (Corey and Hudspeth, 1983;Crawford et al., 1989;Ricci et al., 2005). With our system, we could accurately determine the slow phase of channel activation by fitting the range from 40% to the peak of the rise phase with a single exponential function. When plotted against Po, *dfcr* activation time constants were increased (Fig. 6D). We conclude that in OHCs from *dfcr* mice, resting Po is reduced, and both the kinetics of channel activation and adaptation are slowed.

Discussion

We show here that harmonin, which has previously been linked to inherited forms of deafness in humans, is a component of UTLDs and is required for normal mechanotransduction by cochlear hair cells. Immunogold localization studies show that in hair cells of adult mice, harmonin is concentrated at UTLDs in close proximity to the tip-link protein CDH23. Harmonin localization is affected by a mutation in the PDZ2 domain of harmonin, which disrupts binding to CDH23, and by deletion of the coiled-coil and PST domains, which are required for interactions with F-actin. Although these findings suggest that harmonin interacts at tip links with CDH23 and F-actin, it might also recruit additional proteins to tip links. Hair cells that express a harmonin protein lacking the coiled-coil and PST domains lack UTLDs, indicating that harmonin is essential for UTLD formation. In mice expressing a mutant harmonin protein lacking the coiled-coil and PST domains, tip links are still present and mechanotransduction currents of normal amplitude can be evoked, demonstrating that essential components of the mechanotransduction machinery traffic into stereocilia. However, the properties of mechanotransduction currents of cochlear hair cells are significantly altered in the mutant mice, indicting that harmonin is required for normal mechanotransduction by cochlear hair cells. Interestingly, the mechanotransduction machinery of cochlear hair cells undergoes a stepwise morphological and functional maturation, where sensitivity to mechanical stimuli develops before adaptation (Waguespack et al., 2007). The properties of transducer currents in *dfcr* mice share similarities with those in immature cochlear hair cells, including reduced Po and slowed adaptation, suggesting that harmonin is required for the

maturation of a hair cell's mechanotransduction machinery to achieve optimal sensitivity of the hair bundle to displacement.

Previous studies have shown that harmonin is expressed in developing hair cells, where it is required for hair bundle morphogenesis (Johnson et al., 2003; Lefevre et al., 2008). Harmonin binds PCDH15 and CDH23, both of which are also required for hair bundle morphogenesis, suggesting that harmonin is required for cadherin function during development (Adato et al., 2005; Alagramam et al., 2001a; Boeda et al., 2002; Di Palma et al., 2001; Lefevre et al., 2008; Reiners et al., 2006; Senften et al., 2006; Siemens et al., 2002; Wada et al., 2001; Wilson et al., 2001). In support of this model, hair bundle development was defective in *harmonin-PDZ2*$^{AAA/AAA}$ mice, which carry a harmonin PDZ2 domain mutation disrupting interactions with CDH23. While this mutation also should affect interactions between harmonin and PCDH15, we believe that interactions with CDH23 are the most critical. First, CDH23 and harmonin both change distribution strikingly during hair bundle development. Initially, both proteins are expressed broadly in stereocilia, but they subsequently coalesce to a small region below the tips of stereocilia as bundles mature (Boeda et al., 2002; Kazmierczak et al., 2007; Lagziel et al., 2005; Lefevre et al., 2008; Michel et al., 2005; Rzadzinska et al., 2005; Siemens et al., 2002; Siemens et al., 2004). Second, while the CD1 splice variant of PCDH15 can bind to harmonin, the interaction is of low affinity (Senften et al., 2006), and PCDH15-CD1 and harmonin localize to different regions in hair cells (Ahmed et al., 2006; Senften et al., 2006).

Unexpectedly, the coiled-coil and PST domains of harmonin, which can bundle F-actin in vitro (Boeda et al., 2002), are not essential for hair bundle morphogenesis. As *dfcr* mice were reported to have defects in hair bundle morphology (Johnson et al., 2003), we were surprised that bundle structure was unaffected in our *dfcr* colony, a discrepancy that may be explained by a genetic modifier locus. A genetic modifier might differentially affect the expression of the mutated harmonin gene. For example, an effective mRNA surveillance machinery might eliminate the mutated harmonin mRNA in *dfcr* mice on certain mixed genetic backgrounds, leading in to a null allele. On other genetic backgrounds such as C57Bl/6, mRNA surveillance might be less efficient and lead to the expression of a truncated harmonin protein with partial function. While previous studies were carried out on a mixed genetic background (Johnson et al., 2003), we maintain our *dfcr* colony on an inbred C57Bl/6 background.

We also demonstrate that harmonin is associated with tip links of functionally mature hair cells. Harmonin localizes to the UTLD, where CDH23 inserts into the stereociliary membrane. Although other proteins may control harmonin localization at tip links, we suggest that CDH23 has a critical role. Consistent with this interpretation, harmonin localization was disrupted not only in *harmonin-PDZ2*$^{AAA/AAA}$ mice (this study), but also in CDH23-deficient *waltzer* mice (Lefevre et al., 2008). Another protein that might affect harmonin localization in mature hair cells is PCDH15-CD1, which binds in vitro to harmonin (Adato et al., 2005; Boeda et al., 2002; Reiners et al., 2006; Siemens et al., 2002). However PCDH15-CD1 and harmonin appear to show a distinct distribution in functionally mature hair cells (Ahmed et al., 2006; Senften et al., 2006), although further studies are necessary to clarify this point.

Normal harmonin localization was affected not only in *harmonin-PDZ2*$^{AAA/AAA}$ mice but also in *dfcr* mice, suggesting that the coiled-coil and/or PST domains of harmonin are also important for protein targeting. This result was not necessarily anticipated because PDZ2 of harmonin in *dfcr* mice is still expected to bind to CDH23. Furthermore, while the deletion of the coiled-coil and PST domains affects interactions of harmonin with F- actin, F-actin is distributed too broadly in stereocilia to determine harmonin localization alone. Interactions of harmonin with yet to be identified proteins are likely involved in protein targeting as well. It is also noteworthy that harmonin molecules can oligomerize; the extreme C-terminus of harmonin binds to harmonin-PDZ1, and the second coiled-coil domain binds PDZ1 and PDZ2 (Adato et al.,

2005; Siemens et al., 2002). Because the second coiled-coil domain of harmonin is disrupted by the *dfcr* mutation, homophilic interactions might have been affected, leading to disruption of a cluster of harmonin molecules at UTLDs and their transport to the tips of stereocilia. Single harmonin molecules, which might still be bound to each CDH23 molecule at tip links in *dfcr* mice, likely would have escaped detection. Regardless of the mechanism, UTLDs are disrupted in *dfcr* mice. Interestingly, while UTLDs are absent in *dfcr* mice, our histological and electrophysiological data suggest that tip links still form, demonstrating that UTLDs are not essential for the formation of these filaments.

The localization of harmonin at UTLDs prompted us to determine whether the gating properties of mechanotransduction channels were altered in *dfcr* mice. The amplitudes of saturated transducer currents were unaffected, indicating that the total number of transduction channels was not reduced by the mutation. However, the displacement-Po relationship plot was shifted to the right and broadened, indicating that the mechanotransduction machinery was functionally altered. According to prevailing models of mechanotransduction, excitatory hair bundle deflections increase tension in the gating spring, connected to the transducer channel, leading to rapid channel opening (Corey and Hudspeth, 1983). Tip links have been proposed to be the gating spring or to be in series with it (Pickles et al., 1984). Subsequent to channel opening, channels reclose with slow and fast time constants. Fast adaptation depends on Ca^{2+}, which enters through the channel and binds to a site on or near the channel. Slow adaptation has been most thoroughly studied in vestibular hair cells, where it depends on the motor protein MYO1C, which is thought to control the position of the transduction complex along the length of the stereocilium. As a result of adaptation, channel Po resets towards its resting value, which is near the point of optimal sensitivity along the displacement-Po relationship (Fettiplace and Ricci, 2003; Gillespie and Cyr, 2004; LeMasurier and Gillespie, 2005).

In light of current models of mechanotransduction, the changes in the properties of mechanotransduction currents in *dfcr* mice can be explained plausibly by an effect of harmonin on MYO1C function (Fig. 7). In this model, harmonin directly or indirectly regulates MYO1C motor function, by increasing the number of active motor proteins within the motor complex of each transduction unit, increasing net force production, and by reducing variability in force production by the motor complex. Alternatively, interactions of harmonin with CDH23 and F-actin might optimally align the motor complex relative to the tip link. As a consequence of the harmonin mutation in *dfcr* mice, transduction complexes in different stereocilia of a hair cell produce less force, moreover, the complexes in different stereocilia of a hair cell would be less well coordinated and therefore at a variety of resting positions. In this interpretation, reduced force production leads to a decrease in the average resting Po, and the variability in the response of individual transduction complexes to displacement leads to the broadening of the displacement-Po relationship.

This model also explains the slowed kinetics of channel activation and fast adaptation in OHCs from *dfcr* mice. Previous studies have shown that the kinetics of channel activation is best described by a three-state model, in which each channel passes from one closed state to a second closed state and finally to an open state (Corey and Hudspeth, 1983). In hair cells from *dfcr* mice, average resting tension is reduced, indicating that more channels are in the first closed state. Upon displacement of hair bundles, channel opening will be delayed because a larger fraction of channels must pass through the second closed state before opening. In addition, as a consequence of slowed activation kinetics, fast adaptation in each transduction complex is initiated at different time points, leading to overall slowing of this form of adaptation.

The observation that slow adaptation is also slowed in OHCs cells from *dfcr* mice suggests that harmonin function in hair cells is more complex than our simple model proposes.

According to current models of adaptation, a reduced number of active MYO1C motor proteins in *dfcr* OHCs would have led to faster slipping of the motor complex along the cytoskeleton in response to elevated tension, and therefore to an increased rate of slow adaptation. Perhaps, harmonin not only controls motor activity, but also accelerates motor detachment from the cytoskeleton, facilitating slipping of the motor complex under tension.

It should also be noted that current models of MYO1C function in adaptation are largely based on the study of vestibular hair cells. In agreement with earlier findings (Waguespack et al., 2007), we observed that slow and fast adaptation in rodent cochlear hair cells are an order of magnitude faster than in vestibular hair cells and may well depend on different molecules and mechanisms. An interesting candidate that might be required for harmonin function in hair cells is MYO7A. Harmonin binds to MYO7A (Boeda et al., 2002), and mutations in the *Myo7a* gene affect resting tension in cochlear hair cells (Kros et al., 2002). MYO7A might substitute for MYO1C in auditory hair cells, generating substantially different properties of adaptation in these cells. Finally, harmonin is appropriately localized to regulate interaction of the plasma membrane with the underlying cytoskeleton. UTLDs of wild-type mice are cup shaped with a central indentation facing the plasma membrane (Furness and Hackney, 1985). Neither the UTLDs nor the indentation are present in *dfcr* mice, indicating that membrane curvature at the upper insertion site of tip links is affected by harmonin. Such curvature could significantly change the spatial arrangement of CDH23 and cytoplasmic proteins (e.g. MYO1C) at the upper insertion site of the tip link, their interaction with the membrane, and how they respond to changes in tension.

In summary, we provide here new insights into the mechanisms that regulate mechanotransduction by cochlear hair cells. We demonstrate that harmonin is an integral component of UTLDs, where it is appropriately positioned to regulate mechanotransduction (Fig. 7). In *dfcr* mice, the sensitivity of hair bundles to displacement is reduced, providing evidence that harmonin increases channel activation for small stimuli. Our findings also reinforce the concept that the mechanotransduction machinery of cochlear hair cells is asymmetric, with distinct functions for the upper and lower ends of tip links. This model is supported by the asymmetric distribution of CDH23 and PCDH15 at tip links (Kazmierczak et al. 2007), the localization of harmonin at UTLDs (this manuscript), and the localization of transduction channels at LTLDs (Beurg et al. 2009).

Experimental Procedures

Antibodies and reagents

Anti-harmonin H3 antiserum was raised in rabbits against a GST fusion protein containing the third PDZ domain (amino acids 367 – 541) of harmonin (NCBI accession number AAG12457). Immunizations were carried out at Eurogentec (Brussels, Belgium). Antibodies were affinity purified against harmonin fused to the maltose binding protein as described (Siemens et al., 2002). Additional reagents were: Alexa Fluor 488-phalloidin, Alexa Fluor 594 goat anti-rabbit, TOP-RO3 and Alexa Fluor 647-phalloidin (Invitrogen, Carlsbad, CA), 6 nm colloidal Gold-Affinipure Goat Anti-Rabbit IgG (H+L) (Jackson Immuno Research), 20 nm colloidal Gold Goat Anti-Rabbit IgG (H+L) (Ted Pella).

Transfections, immunocytochemistry, Western blot analysis, and whole mount staining

A pCDNA expression vector (Invitrogen) containing a cDNA encoding a harmonin-GFP fusion protein was transfected into Hela cells using Fugene 6 (Roche Diagnostics Corporation, Indianapolis, IN). Immunocytochemistry, Western-blot analysis and cochlear whole mount staining were carried out as described (Senften et al., 2006).

Immunogold electron microscopy

All experiments involving animals and the maintenance of animals were carried out in accordance with institutional guidelines. Animals were anesthetized and perfused with 4% PFA, 0.025% glutaraldehyde in Na-cacodylate 0.1 M, pH 7.4, 0.025% picric acid. The cochlear shell was opened and incubated in the same fixative for 1 h. Tissue was washed with Tris-buffered saline (TBS, 150 mM NaCl, 10 mM Tris-HCl) pH 7.6, and the cochlear shell, Reissner's membrane and tectorial membrane were removed. Tissue was blocked for 1 h at room temperature in TBS containing 4% BSA and 0.02% Triton X-100, and incubated over night at 4°C with anti-harmonin H3 antibody in TBS containing 1% BSA and 0.02% Triton X-100. Tissue was washed in TBS and incubated for 2 days at 4°C with anti-rabbit antibody conjugated with colloidal gold beads. Tissue was washed in TBS and 0.1M Na-cacodylate, and post-fixed for 24 h at 4°C with 2.5 % glutaraldehyde in 0.1 M Na-cacodylate. Decalcification of the modiolus was performed by adding 1:3 Vol/Vol 0.5 M EDTA, pH 8.0 to fixative and incubation for 3 h at 4°C. Tissue was washed with 0.1 M Na-cacodylate and post-fixed for 1.5 h in 1% OsO4 in 0.1 M Na-Cacodylate, washed, dehydrated and cleared in propylene oxide. Tissue was impregnated in Epon/Araldite resin and the organ of Corti further microdissected and samples polymerized at 60°C. Thick sections were initially taken to assess the orientation. Thin sections were cut, post-stained for 30 min with uranyl acetate followed by 20 min incubation in lead citrate. Grids were examined on a Philips CM100 electron microscope (FEI, Hillsbrough, OR). Images were documented using Kodak S0163 EM film. Negatives were scanned at 605 Ipi using a Fuji FineScan 2750xl (Hemel, Hempstead, Herts, UK).

Analysis of tip-link densities

Tissues were fixed for 1 h in 4% PFA, 2.5% glutaraldehyde in Na-cacodylate 0.1 M, pH 7.4, 0.025% picric acid, microdissected to expose the cochlea, further fixed for 1 day at 4°C, decalcified and treated as described above. Tissue was impregnated in Epon/Araldite resin and baked at 60°C. 10 nm sections were post-stained for 30 min with uranyl acetate and for 20 min with lead, and analyzed as described above. Each block was processed by sets of 7–8 consecutive thin sections spaced by 8 μm trimming.

Generation of *harmonin-PDZ2*AAA* mice

The knock-in construct is shown in Supplementary Fig. 2. Genomic DNA from 129/Sv mice was used to PCR a fragment of *USH1C* genomic DNA ~6.5 kb long (Long Template PCR – Roche). The GLG motif (221 – 223) in the PDZ2 domain was mutated to AAA also creating a NotI restriction site in exon 8 (nucleotides 687 – 694). A pGK-neomycin resistance cassette flanked by recognition sites for FLP recombinase was inserted into the intron between exon 6 and 7. The linearized targeting construct was electroporated into SvEv CCE mouse ES cells, G418-resistant colonies with the correct targeting event were identified and injected into C57Bl/6 blastocysts. The resulting chimeras were mated with C57Bl/6 females. Germline transmission of the mutated allele was confirmed in the offspring by PCR analysis and NotI restriction digestion. Chimeric mice were mated with 6JSJL-Tg Flp deleter mice (Jackson Laboratory, Bar Harbor, ME) to remove the pGK-neo cassette. Primers flanking the FRT-loxP sites were used for genotyping mutants: sense 5′-CCTGAACTTGCACTGCTCCT-3′; antisense 5′-CCAGGTACCCTAGTGACCTATG-3′ (264 bp wild type allele; 332 bp mutant allele). The following primers were used to amplify a 1170 bp product from P5 cochlea cDNA to confirm the presence of the mutation in cDNA from the inner ear of mutant mice: sense 5′-GGCCCGAGAATTCCGACACA-3′; antisense 5′-TGCACCTCTGCGGTGATGG-3′.

Cochlear preparation and recordings

P7-P8 mice were sacrificed by decapitation. The first postnatal day is counted as P0. The organ of Corti was dissected as described for rats (Ricci et al., 2005) with little modification. Briefly,

the inner ear was transferred to a chamber with dissection solution (in mM): 141.7 NaCl, 5.36 KCl, 1 $MgCl_2$, 0.5 $MgSO_4$, 0.1 $CaCl_2$, 3.4 L-Glutamine, 10 glucose and 10 H-HEPES, pH 7.4. The bony capsule was opened to expose the cochlea and the stria vascularis and tectorial membrane were removed. The cochlear coil was fixed in a recording chamber with glass bottom. The recording chamber was perfused with WPI Peri-Star peristaltic pump (World Precision Instrument, Sarasota, Florida) with artificial perilymph (in mM): 144 NaCl, 0.7 NaH_2PO_4, 5.8 KCl, 1.3 $CaCl_2$, 0.9 $MgCl_2$, 5.6 glucose, and 10 H- HEPES, pH 7.4. Cells were observed with an Olympus BX51WI microscope mounted with a 60X water-immersion objective and Qimaging ROLERA-RX camera (Qimaging, Canada) with 2X optic extender (Edmund, Barrington, NJ). OHCs in the apical and apical-middle turns were recorded at room temperature (19 –22°C). Patch pipettes were pulled with Sutter P-97 (Sutter instrument, Novato, CA) and polished with MF-830 microforge (Narishige, East Meadow, NY) with resistances of 1.5–2 MΩ from borosilicate glass with filament (Sutter instrument, Novato, CA), filled with intracellular solution (in mM): 140 KCl, 1 $MgCl_2$, 0.1 EGTA, 2 Mg-ATP, 0.3 Na-GTP and 10 H-HEPES, pH7.2. Cells were whole-cell patched for recoding mechanotransduction currents at −70 mV holding potential with an Axopatch 200B (Molecular Devices, Sunnyvale, CA) or an EPC 10 USB (HEKA instruments, Bellmore, New York) patch-clamp amplifier. Transduction currents were digitized ≥ 20 KHz with Digidata 1440A AD/DA converter and pClamp 10.0 software (Molecular Devices, Sunnyvale, CA), or Patchmaster 2.35 softeware (HEKA instruments, Bellmore, NY). Usually, recordings were made in the first row of OHCs. And each preparation was recorded within 1 hour.

Hair bundle stimulation

For mechanical stimulation, hair bundles were deflected with a glass probe mounted on a piezoelectric stack actuator (model P-885, Physik Instrument, Karlsruhe, Germany). The tip of the pipette was fire-polished to about 3 μm diameter to fit the “V” shape of hair bundle of OHCs (apical-middle coil). The tip of the probe was cleaned in chromic acid to allow adherence to hair bundle. The actuator was driven with voltage steps that were low-pass filtered with an eight-pole Bessel filter (model 900CT, Frequency Devices Ottawa, IL) at 5 KHz frequency to diminish the resonance of the piezo stack. The output driving voltage to the piezo stack was monitored by oscilloscope to ensure the rise time was less than 100 ms. The deflection of piezo stack was calibrated with an Olympus IX70 microscope equipped with a 100X oil-immersion objective (NA 1.3) and a Hamamatsu Orca ER-II camera (Hamamatsu Photonics, Bridgewater, NJ) with a resolution of 1344×1024 pixels. In brief, the electrode with 0.1 μm tip was fixed to the piezo stack. Then the movements induced by certain driving voltage were measured and plotted to calculate the slope. The microscopy system was calibrated with a stage-micrometer and operated by Metamorph software (Molecular Devices, Sunnyvale, CA).

Analysis

Data analysis was performed using Igor pro 6 software (WaveMetrics, Lake Oswego, OR) integrated with Neuromatic analysis package. To calculate the channel open probability (P_o), I(X) curves in Fig. 5B were fitted with second-order Boltzmann equation: $I(X) = I_{min} - I_{max}/((1+e^{z2(x-x2)})(1+e^{z1(x-x1)}))$, where I_{min} and I_{max} are the minimum and maximum current; z_2 and z_1 are the slope of the curve; and x_2 and x_1 are the position of the curve along the x-axis (Stauffer and Holt, 2007). The equation was also used to fit the data in Fig. 5C and 6D. The current adaptation time constants were fitted with second-order exponential equation: $I = I_0 + A_1e^{-t/\tau 1} + A_2e^{-t/\tau 2}$. Data are shown as mean ± SEM. Student’s two-tailed unpaired *t* test was used to determine statistical significance (*, $p<0.05$, **, $p<0.01$, ***, $p<0.001$).

Auditory brainstem responses (ABR)

Measurements of the ABRs were performed using a TDT workstation (Tucker Davis Technologies Inc. U.S.A.) as described (Schwander et al., 2007).

Supplementary Material

Refer to Web version on PubMed Central for supplementary material.

Acknowledgments

We thank Anthony Ricci for help with electrophysiology and for comments on the manuscript; C. Ramos, G. Martin and S. Kupriyanov for assistance in generating mice; K. Spencer, M. Wood and T. Fassel for help with microscopy and EM. This work was funded by NIH grants DC005969, DC007704 (U.M), EYE07042 (D.W.), DC002368 (P.G.), the Skaggs Institute for Chemical Biology (U.M.), a Jules and Doris Stein RPB professorship (D.W.), a C.J. Martin fellowship (#148939) NHMRC (Australia) (A.R.), and a fellowship from the Bruce Ford and Anne Smith Bundy Foundation (A.R., W.X).

References

Adato A, Michel V, Kikkawa Y, Reiners J, Alagramam KN, Weil D, Yonekawa H, Wolfrum U, El-Amraoui A, Petit C. Interactions in the network of Usher syndrome type 1 proteins. Hum Mol Genet 2005;14:347–356. [PubMed: 15590703]

Ahmed ZM, Goodyear R, Riazuddin S, Lagziel A, Legan PK, Behra M, Burgess SM, Lilley KS, Wilcox ER, Riazuddin S, et al. The tip-link antigen, a protein associated with the transduction complex of sensory hair cells, is protocadherin-15. J Neurosci 2006;26:7022–7034. [PubMed: 16807332]

Ahmed ZM, Riazuddin S, Bernstein SL, Ahmed Z, Khan S, Griffith AJ, Morell RJ, Friedman TB, Wilcox ER. Mutations of the protocadherin gene PCDH15 cause Usher syndrome type 1F. Am J Hum Genet 2001;69:25–34. [PubMed: 11398101]

Ahmed ZM, Smith TN, Riazuddin S, Makishima T, Ghosh M, Bokhari S, Menon PS, Deshmukh D, Griffith AJ, Friedman TB, Wilcox ER. Nonsyndromic recessive deafness DFNB18 and Usher syndrome type IC are allelic mutations of USHIC. Hum Genet 2002;110:527–531. [PubMed: 12107438]

Alagramam KN, Murcia CL, Kwon HY, Pawlowski KS, Wright CG, Woychik RP. The mouse Ames waltzer hearing-loss mutant is caused by mutation of Pcdh15, a novel protocadherin gene. Nat Genet 2001a;27:99–102. [PubMed: 11138007]

Alagramam KN, Yuan H, Kuehn MH, Murcia CL, Wayne S, Srisailpathy CR, Lowry RB, Knaus R, Van Laer L, Bernier FP, et al. Mutations in the novel protocadherin PCDH15 cause Usher syndrome type 1F. Hum Mol Genet 2001b;10:1709–1718. [PubMed: 11487575]

Assad JA, Shepherd GM, Corey DP. Tip-link integrity and mechanical transduction in vertebrate hair cells. Neuron 1991;7:985–994. [PubMed: 1764247]

Belyantseva IA, Boger ET, Naz S, Frolenkov GI, Sellers JR, Ahmed ZM, Griffith AJ, Friedman TB. Myosin-XVa is required for tip localization of whirlin and differential elongation of hair-cell stereocilia. Nat Cell Biol 2005;7:148–156. [PubMed: 15654330]

Beurg M, Fettiplace R, Nam JH, Ricci T. Localization of inner hair cell mechanotransducer channels using high speed calcium imaging. Nat Neuroscience. 2009in press

Boeda B, El-Amraoui A, Bahloul A, Goodyear R, Daviet L, Blanchard S, Perfettini I, Fath KR, Shorte S, Reiners J, et al. Myosin VIIa, harmonin and cadherin 23, three Usher I gene products that cooperate to shape the sensory hair cell bundle. Embo J 2002;21:6689–6699. [PubMed: 12485990]

Bolz H, von Brederlow B, Ramirez A, Bryda EC, Kutsche K, Nothwang HG, Seeliger M, del CSCM, Vila MC, Molina OP, et al. Mutation of CDH23, encoding a new member of the cadherin gene family, causes Usher syndrome type 1D. Nat Genet 2001;27:108–112. [PubMed: 11138009]

Bork JM, Peters LM, Riazuddin S, Bernstein SL, Ahmed ZM, Ness SL, Polomeno R, Ramesh A, Schloss M, Srisailpathy CR, et al. Usher syndrome 1D and nonsyndromic autosomal recessive deafness DFNB12 are caused by allelic mutations of the novel cadherin-like gene CDH23. Am J Hum Genet 2001;68:26–37. [PubMed: 11090341]

Corey DP, Hudspeth AJ. Kinetics of the receptor current in bullfrog saccular hair cells. J Neurosci 1983;3:962–976. [PubMed: 6601694]

Crawford AC, Evans MG, Fettiplace R. Activation and adaptation of transducer currents in turtle hair cells. J Physiol 1989;419:405–434. [PubMed: 2621635]

Delprat B, Michel V, Goodyear R, Yamasaki Y, Michalski N, El-Amraoui A, Perfettini I, Legrain P, Richardson G, Hardelin JP, Petit C. Myosin XVa and whirlin, two deafness gene products required for hair bundle growth, are located at the stereocilia tips and interact directly. Hum Mol Genet 2005;14:401–410. [PubMed: 15590698]

Di Palma F, Holme RH, Bryda EC, Belyantseva IA, Pellegrino R, Kachar B, Steel KP, Noben-Trauth K. Mutations in Cdh23, encoding a new type of cadherin, cause stereocilia disorganization in waltzer, the mouse model for Usher syndrome type 1D. Nat Genet 2001;27:103–107. [PubMed: 11138008]

Fettiplace R, Ricci AJ. Adaptation in auditory hair cells. Curr Opin Neurobiol 2003;13:446–451. [PubMed: 12965292]

Furness DN, Hackney CM. Cross-links between stereocilia in the guinea pig cochlea. Hear Res 1985;18:177–188. [PubMed: 4044419]

Gillespie PG, Cyr JL. Myosin-1c, the hair cell's adaptation motor. Annu Rev Physiol 2004;66:521–545. [PubMed: 14977412]

Johnson KR, Gagnon LH, Webb LS, Peters LL, Hawes NL, Chang B, Zheng QY. Mouse models of USH1C and DFNB18: phenotypic and molecular analyses of two new spontaneous mutations of the Ush1c gene. Hum Mol Genet 2003;12:3075–3086. [PubMed: 14519688]

Kazmierczak P, Sakaguchi H, Tokita J, Wilson-Kubalek EM, Milligan RA, Muller U, Kachar B. Cadherin 23 and protocadherin 15 interact to form tip-link filaments in sensory hair cells. Nature 2007;449:87–91. [PubMed: 17805295]

Kennedy HJ, Evans MG, Crawford AC, Fettiplace R. Fast adaptation of mechanoelectrical transducer channels in mammalian cochlear hair cells. Nat Neurosci 2003;6:832–836. [PubMed: 12872124]

Kros CJ, Marcotti W, van Netten SM, Self TJ, Libby RT, Brown SD, Richardson GP, Steel KP. Reduced climbing and increased slipping adaptation in cochlear hair cells of mice with Myo7a mutations. Nat Neurosci 2002;5:41–47. [PubMed: 11753415]

Lagziel A, Ahmed ZM, Schultz JM, Morell RJ, Belyantseva IA, Friedman TB. Spatiotemporal pattern and isoforms of cadherin 23 in wild type and waltzer mice during inner ear hair cell development. Dev Biol 2005;280:295–306. [PubMed: 15882574]

Lefevre G, Michel V, Weil D, Lepelletier L, Bizard E, Wolfrum U, Hardelin JP, Petit C. A core cochlear phenotype in USH1 mouse mutants implicates fibrous links of the hair bundle in its cohesion, orientation and differential growth. Development 2008;135:1427–1437. [PubMed: 18339676]

LeMasurier M, Gillespie PG. Hair-cell mechanotransduction and cochlear amplification. Neuron 2005;48:403–415. [PubMed: 16269359]

Manor U, Kachar B. Dynamic length regulation of sensory stereocilia. Semin Cell Dev Biol 2008;19:502–510. [PubMed: 18692583]

Michel V, Goodyear RJ, Weil D, Marcotti W, Perfettini I, Wolfrum U, Kros CJ, Richardson GP, Petit C. Cadherin 23 is a component of the transient lateral links in the developing hair bundles of cochlear sensory cells. Dev Biol 2005;280:281–294. [PubMed: 15882573]

Muller U. Cadherins and mechanotransduction by hair cells. Curr Opin Cell Biol. 2008

Ouyang XM, Xia XJ, Verpy E, Du LL, Pandya A, Petit C, Balkany T, Nance WE, Liu XZ. Mutations in the alternatively spliced exons of USH1C cause non-syndromic recessive deafness. Hum Genet 2002;111:26–30. [PubMed: 12136232]

Pickles JO, Comis SD, Osborne MP. Cross-links between stereocilia in the guinea pig organ of Corti, and their possible relation to sensory transduction. Hear Res 1984;15:103–112. [PubMed: 6436216]

Reiners J, Nagel-Wolfrum K, Jurgens K, Marker T, Wolfrum U. Molecular basis of human Usher syndrome: deciphering the meshes of the Usher protein network provides insights into the pathomechanisms of the Usher disease. Exp Eye Res 2006;83:97–119. [PubMed: 16545802]

Ricci AJ, Kennedy HJ, Crawford AC, Fettiplace R. The transduction channel filter in auditory hair cells. J Neurosci 2005;25:7831–7839. [PubMed: 16120785]

Rzadzinska AK, Derr A, Kachar B, Noben-Trauth K. Sustained cadherin 23 expression in young and adult cochlea of normal and hearing-impaired mice. Hear Res. 2005

Schwander M, Sczaniecka A, Grillet N, Bailey JS, Avenarius M, Najmabadi H, Steffy BM, Federe GC, Lagler EA, Banan R, et al. A forward genetics screen in mice identifies recessive deafness traits and reveals that pejvakin is essential for outer hair cell function. J Neurosci 2007;27:2163–2175. [PubMed: 17329413]

Senften M, Schwander M, Kazmierczak P, Lillo C, Shin JB, Hasson T, Geleoc GS, Gillespie PG, Williams D, Holt JR, Muller U. Physical and functional interaction between protocadherin 15 and myosin VIIa in mechanosensory hair cells. J Neurosci 2006;26:2060–2071. [PubMed: 16481439]

Sheng M, Sala C. PDZ domains and the organization of supramolecular complexes. Annu Rev Neurosci 2001;24:1–29. [PubMed: 11283303]

Siemens J, Kazmierczak P, Reynolds A, Sticker M, Littlewood-Evans A, Muller U. The Usher syndrome proteins cadherin 23 and harmonin form a complex by means of PDZ-domain interactions. Proc Natl Acad Sci U S A 2002;99:14946–14951. [PubMed: 12407180]

Siemens J, Lillo C, Dumont RA, Reynolds A, Williams DS, Gillespie PG, Muller U. Cadherin 23 is a component of the tip link in hair-cell stereocilia. Nature 2004;428:950–955. [PubMed: 15057245]

Stauffer EA, Holt JR. Sensory transduction and adaptation in inner and outer hair cells of the mouse auditory system. J Neurophysiol 2007;98:3360–3369. [PubMed: 17942617]

Stauffer EA, Scarborough JD, Hirono M, Miller ED, Shah K, Mercer JA, Holt JR, Gillespie PG. Fast adaptation in vestibular hair cells requires Myosin-1c activity. Neuron 2005;47:541–553. [PubMed: 16102537]

Verpy E, Leibovici M, Zwaenepoel I, Liu XZ, Gal A, Salem N, Mansour A, Blanchard S, Kobayashi I, Keats BJ, et al. A defect in harmonin, a PDZ domain-containing protein expressed in the inner ear sensory hair cells, underlies Usher syndrome type 1C. Nat Genet 2000;26:51–55. [PubMed: 10973247]

Vollrath MA, Kwan KY, Corey DP. The micromachinery of mechanotransduction in hair cells. Annu Rev Neurosci 2007;30:339–365. [PubMed: 17428178]

Wada T, Wakabayashi Y, Takahashi S, Ushiki T, Kikkawa Y, Yonekawa H, Kominami R. A point mutation in a cadherin gene, Cdh23, causes deafness in a novel mutant, Waltzer mouse niigata. Biochem Biophys Res Commun 2001;283:113–117. [PubMed: 11322776]

Waguespack J, Salles FT, Kachar B, Ricci AJ. Stepwise morphological and functional maturation of mechanotransduction in rat outer hair cells. J Neurosci 2007;27:13890–13902. [PubMed: 18077701]

Wilson SM, Householder DB, Coppola V, Tessarollo L, Fritzsch B, Lee EC, Goss D, Carlson GA, Copeland NG, Jenkins NA. Mutations in Cdh23 cause nonsyndromic hearing loss in waltzer mice. Genomics 2001;74:228–233. [PubMed: 11386759]

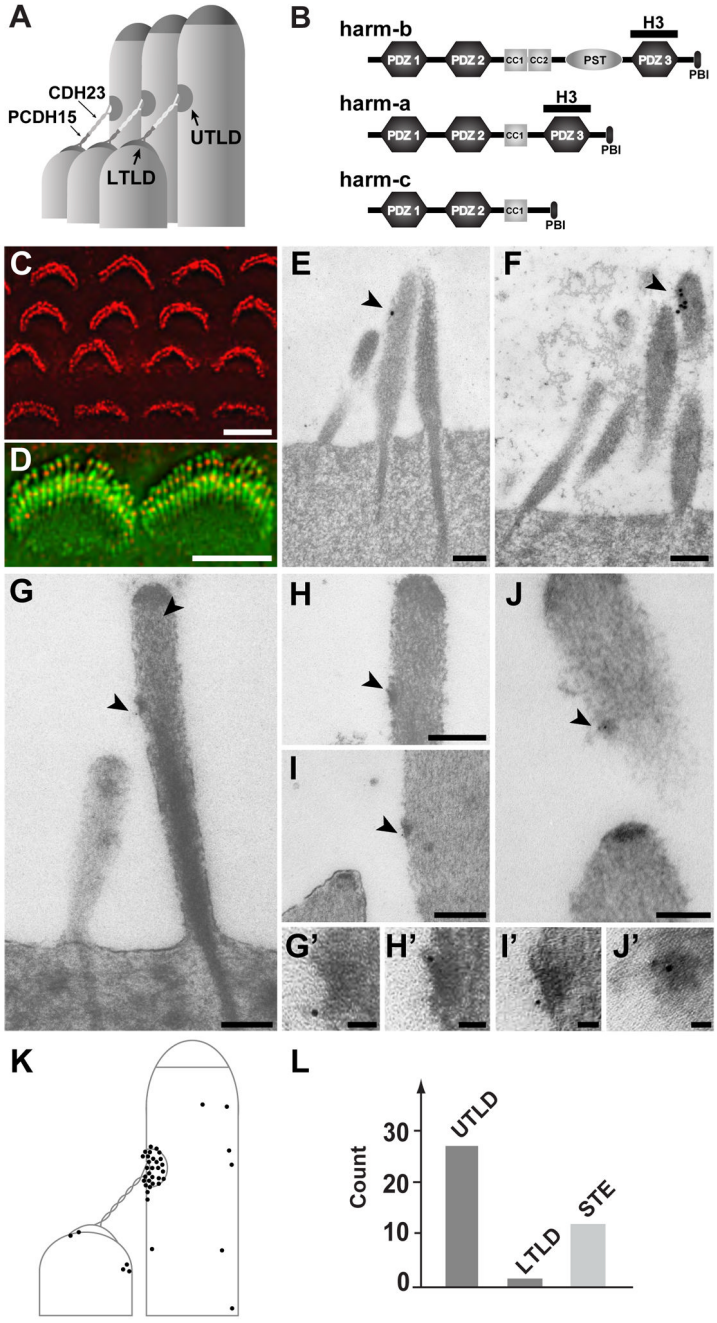

Fig. 1.

Harmonin is localized at UTLDs. (**A**) Diagram of stereociliary tips showing tip links (consisting of PCDH15 and CDH23) terminating in UTLDs and LTLDs. (**B**) Diagram showing the three major harmonin isoforms. The PDZ, coiled-coil (CC), proline-serine-threonine-rich (PST) domain, and binding site for PDZ domains (PBI) are indicated. The H3 antibody was generated against a fragment of harmonin encompassing the PDZ3 domain. (**C**) Immunofluorescence analysis revealed harmonin expression (red) in the stereocilia of P2 cochlear hair cells. (**D**) Higher resolution images of cochlear inner hair cells at P5 stained for harmonin (red) and F-actin (green), showing harmonin localization below stereociliary tips. (**E, F**) Immunogold localization with cochlear hair cells at P5 confirmed harmonin localization below stereociliary

tips (20 nm gold beads). (**G**–**J**) Immunogold localization studies of cochlear hair cells at P35 revealed harmonin localization at UTLDs (arrows) (6 nm gold beads). Panel (**I**) shows an inner hair cell, the other panels outer hair cells. (**G′–J′**) Higher magnification views of the UTLDs shown in panel G to J. (**K**) Distribution of gold particles at P35 as determined in 16 pairs of stereocilia. (**L**) Quantification of gold particles. STE, stereocilia. Scale bars: (C, D) 5 μm; (E–J) 200 nm; (G′ to J′) 25 nm.

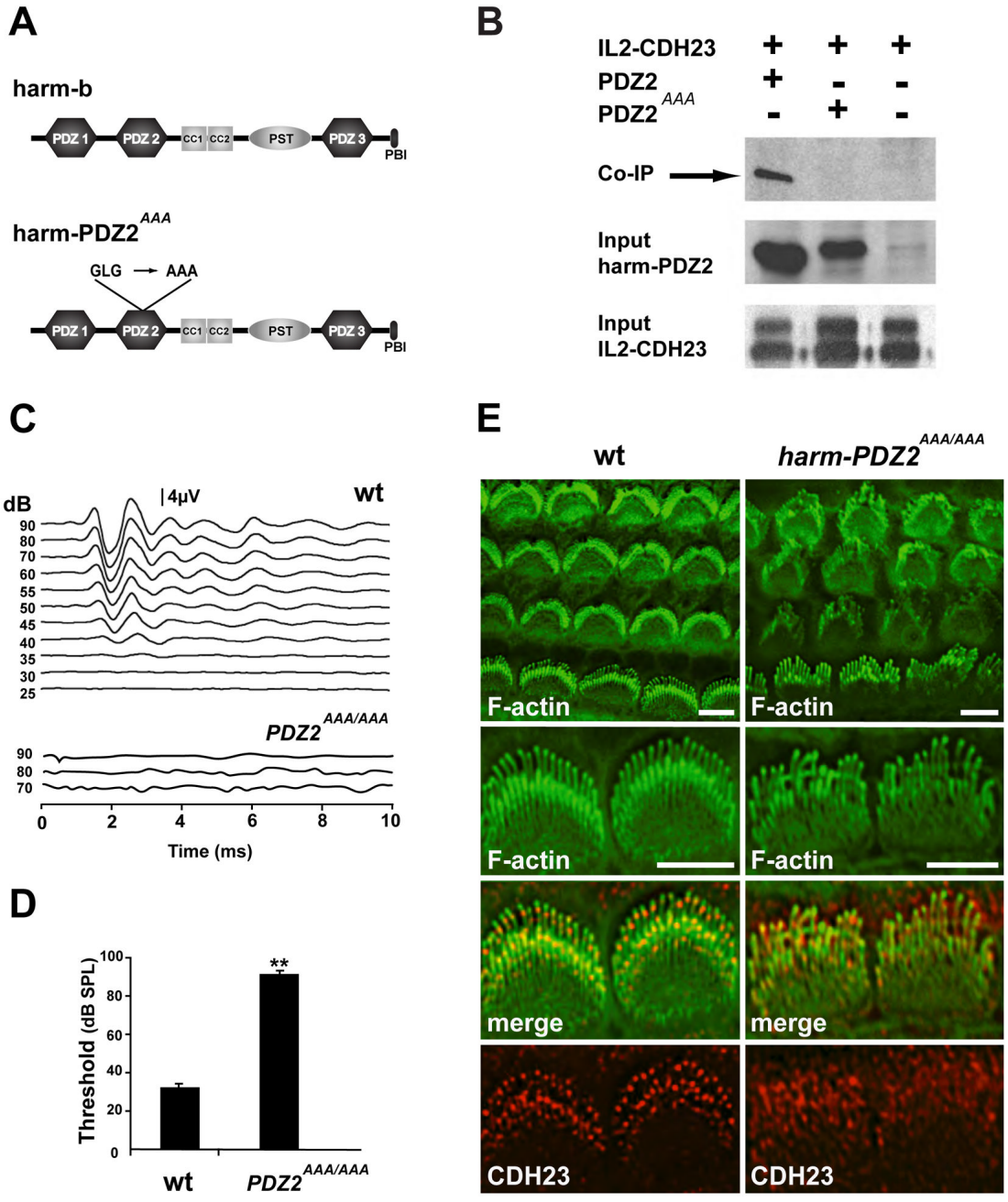

Fig. 2.

Harmonin-PDZ2$^{AAA/AAA}$ mice are deaf and show defects in hair bundle morphology. (**A**) Diagram of harmonin-b protein indicating the mutations in *harmonin-PDZ2*^{AAA}. A critical GLG motif in PDZ2 was changed to AAA. (**B**) HEK cells were transfected to express IL2-CDH23 and the PDZ2 domain of harmonin (with or without the AAA mutation). Upper panel: extracts were used for immunoprecipitation (IP) experiments with antibodies specific to IL2. Proteins were separated by SDS-PAGE and visualized by Western blotting (WB) with an antibody to the PDZ2 domain of harmonin. Note that only the wild-type PDZ2 domain co-immunoprecipitated with IL2-CDH23. Middle and lower panels: as a loading control, proteins were separated by SDS-PAGE without immunoprecipitation, and visualized by Western

blotting with antibodies to the PDZ2 domain of harmonin or to IL2. (**C**) Representative auditory brain stem response traces to click stimuli for wild-type (wt) and *harmonin-PDZ2*$^{AAA/AAA}$ (*PDZ*$^{AAA/AAA}$) mice at 4 weeks of age. (**D**) ABR thresholds in 4 week old mice (wild type +/+ $n = 4$; homozygous mutants −/− $n = 6$; mean ± SEM **P < 0.01, Student's *t*-test). (**E**) Cochlear whole mounts at P5 were stained to reveal F-actin (green) and harmonin (red). Hair bundle morphology was disrupted in *harmonin-PDZ2*$^{AAA/AAA}$ mice. Harmonin was widely distributed in stereocilia of *harmonin-PDZ2*$^{AAA/AAA}$ mice. Scale bars: (E) 5 μm.

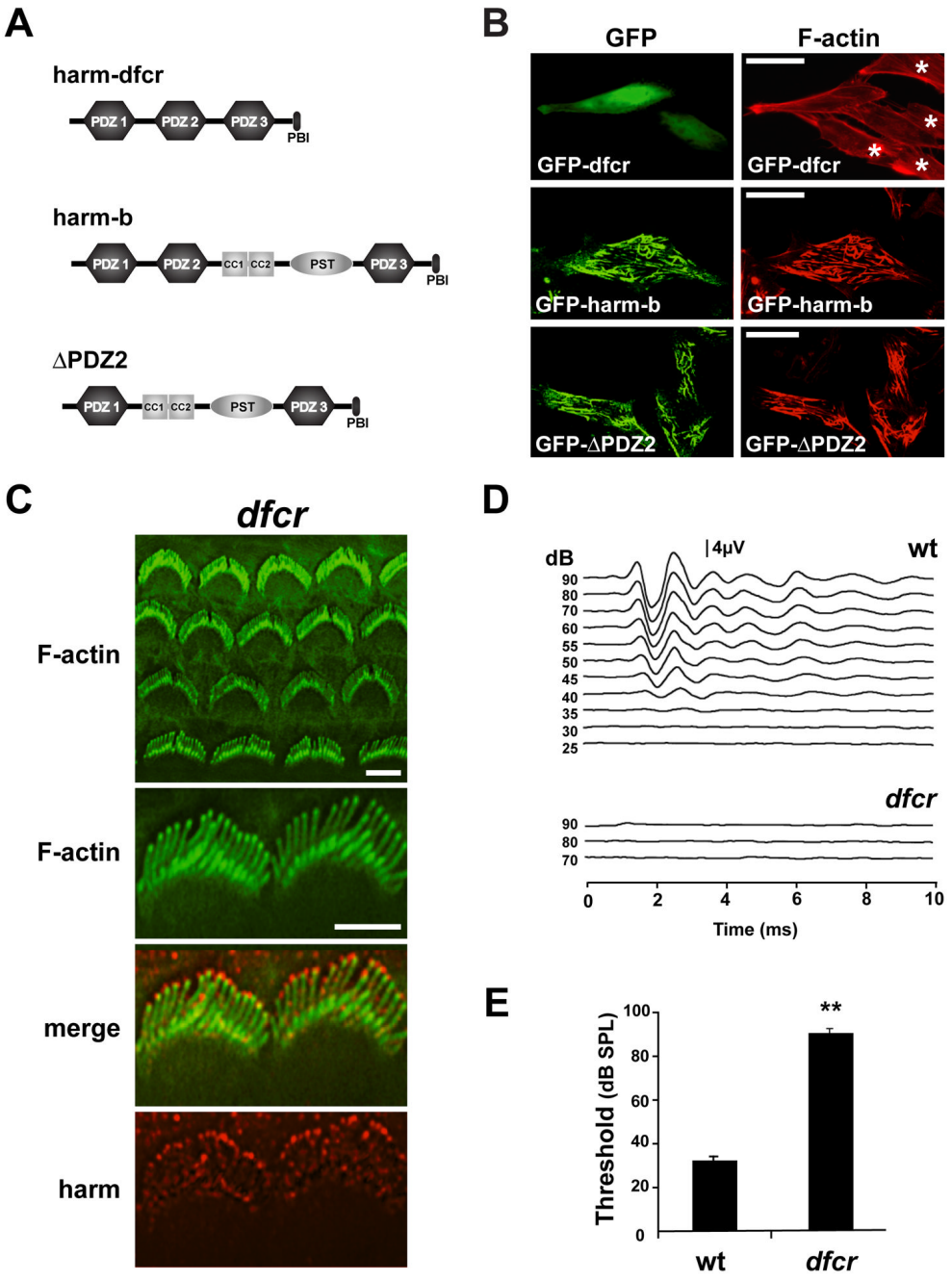

Fig. 3.

Dfcr mice are deaf but show no defects in hair bundle morphology. (**A**) Diagram of (i) the truncated harmonin protein that is expressed in *dfcr* mice, (ii) harmonin-b, (iii) ΔPDZ-harmonin-b (ΔPDZ), which was engineered to lack PDZ2. (**B**) The three harmonin variants shown in (A) were fused to EGFP and expressed by transfection in Hela cells. Harmonin variants were visualized by EGFP fluorescence, and the F-actin cytoskeleton was labeled with rhodamine-phalloidine. GFP-dfcr was diffusely expressed in cells, while GFP-harmonin-b and GFP-harmonin-b ΔPDZ were associated with F-actin filaments. Note that F-actin filaments in untransfected cells (asterisks in the upper right panel) and in cells expressing GFP-dfcr formed far fewer and thinner F-actin bundles when compared to cells expressing GFP-harmonin-b or

GFP-harmonin-b DPDZ. (**C**) Cochlear whole mounts of *dfcr* mice at P5 were stained to reveal F-actin (green) and harmonin (red). Hair bundle morphology was maintained in *dfcr* mice, but harmonin was mislocalized to the very tips of stereocilia. (D) Representative auditory brain stem response traces to click stimuli for wild type (wt) and *dfcr* mice at 4 weeks of age. (E) ABR thresholds in 4 week old mice (wild type +/+ $n = 5$; homozygous mutants −/− $n = 6$; mean ± SEM **P < 0.01, Student's *t*-test). Scale bars: (B) 20 μm;(C) 5 μm.

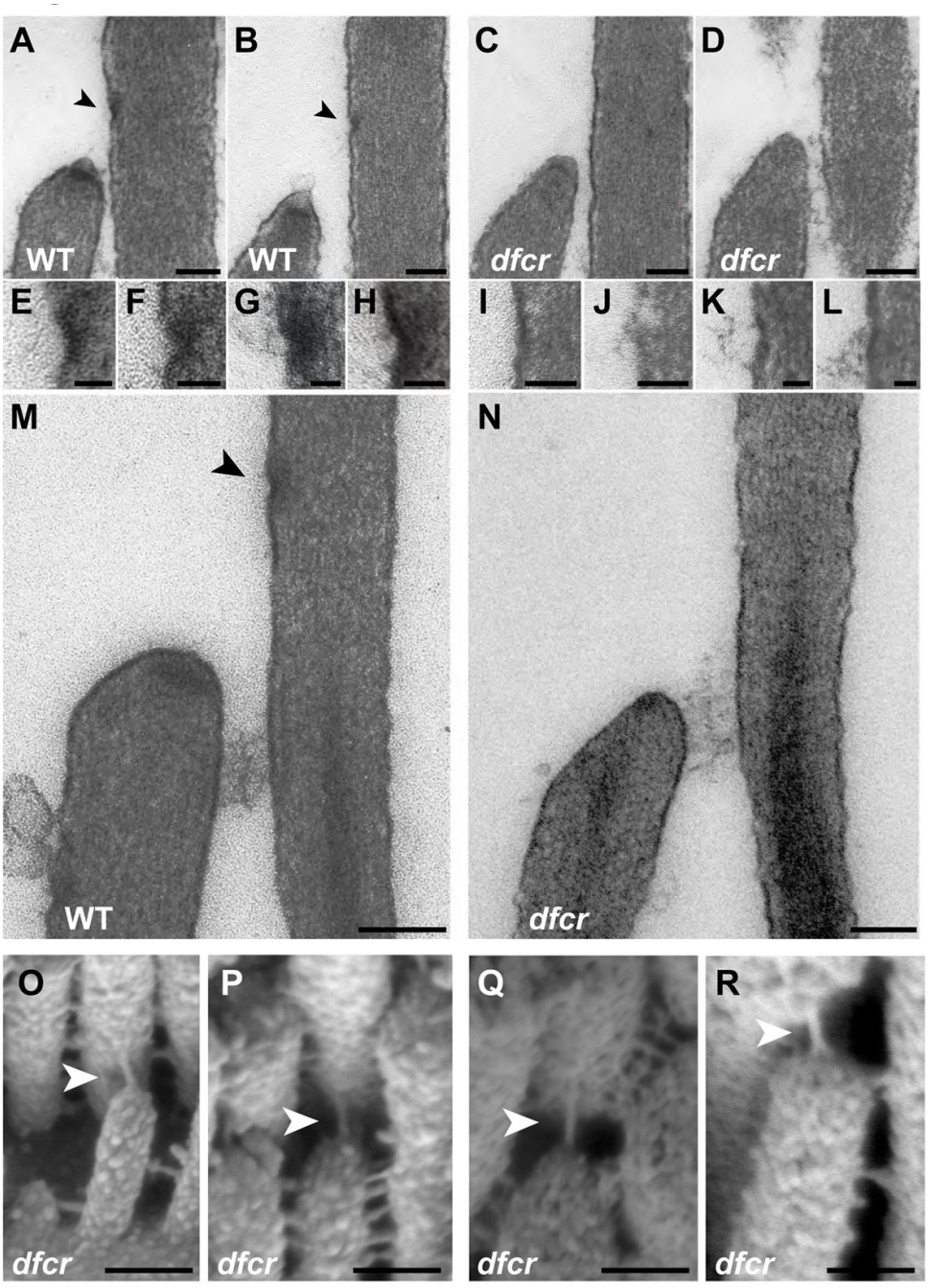

Fig. 4.

Hair bundles in the cochlea of *dfcr* mice lack UTLDs but contain tip links. (**A**–**D**) Sections through stereocilia of OHCs at P10. The tenting of stereociliary tips was detectable in wild-type littermates (A,B) and mutant mice (C,D); tip-link filaments projecting from the tips of stereocilia to the side of the next taller stereocilium were just visible. Arrowheads mark UTLDs. (**E**–**H**) Higher magnification views of UTLDs in wild-type mice showing the characteristic cup shape and indentation at the membrane. (**I**–**L**) UTLDs were not observed in *dfcr* mice. (**M**, **N**) Stereocilia at P70. The UTLD was clearly visible in wild-type littermates, but absent in homozygous *dfcr* mice. (0–R) Scanning electron micrographs of cochlear hair cells at P12. Tip links are indicated by arrowheads. Scale bars: (A–D, M,N) 100 nm; (E–L) 50 nm.

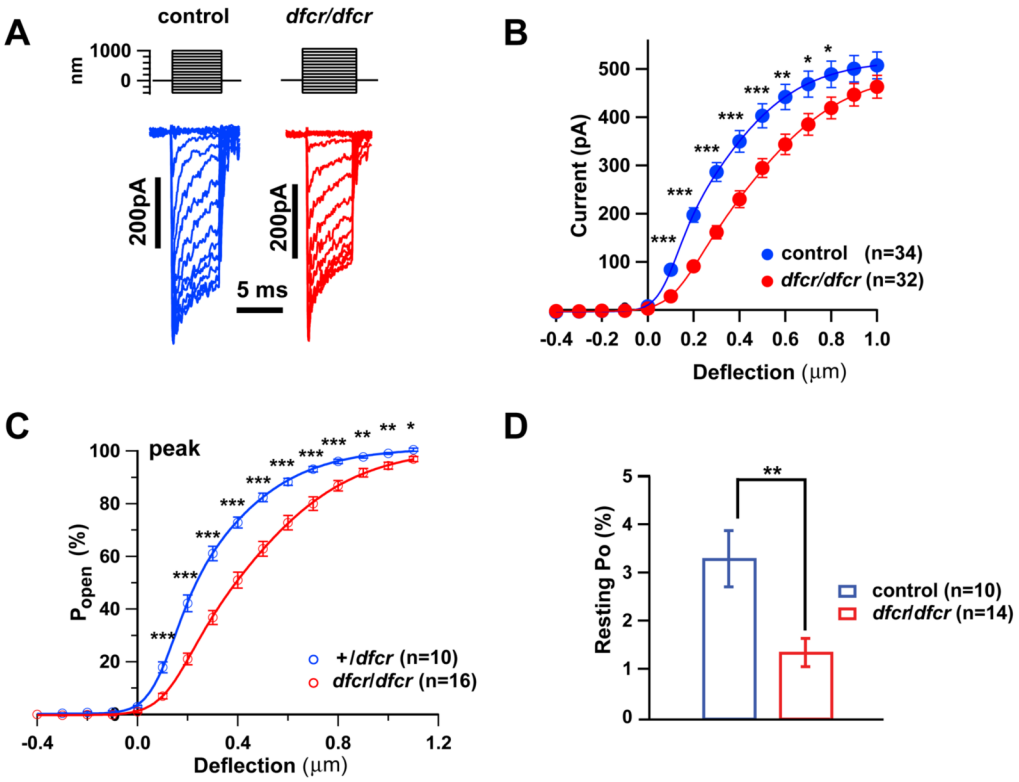

Fig. 5.

Analysis of mechanotransduction currents in OHCs from *dfcr* mice. In all panels, data from hair cells of wild-type mice are represented in blue and from homozygous *dfcr* mice in red. (**A**) Examples of transduction currents in OHCs at P7–P8 in response to 5 ms mechanical stimulation. (**B**) Current-displacement [I(X)] relationships were plotted and fitted with a second-order Boltzmann function. Peak currents at maximal deflection were similar in OHCs from wild-types and mutants. (**C**) The Po-displacement relationship plot obtained with peak currents following deflection reveals a significant rightward shift and broadening of the curve in mutants. (**D**) The resting Po was significantly reduced in the mutants. All data are shown as mean ± SEM. Student's two-tailed unpaired *t* test was used to determine statistical significance (*, $p<0.05$, **, $p<0.01$, ***, $p<0.001$).

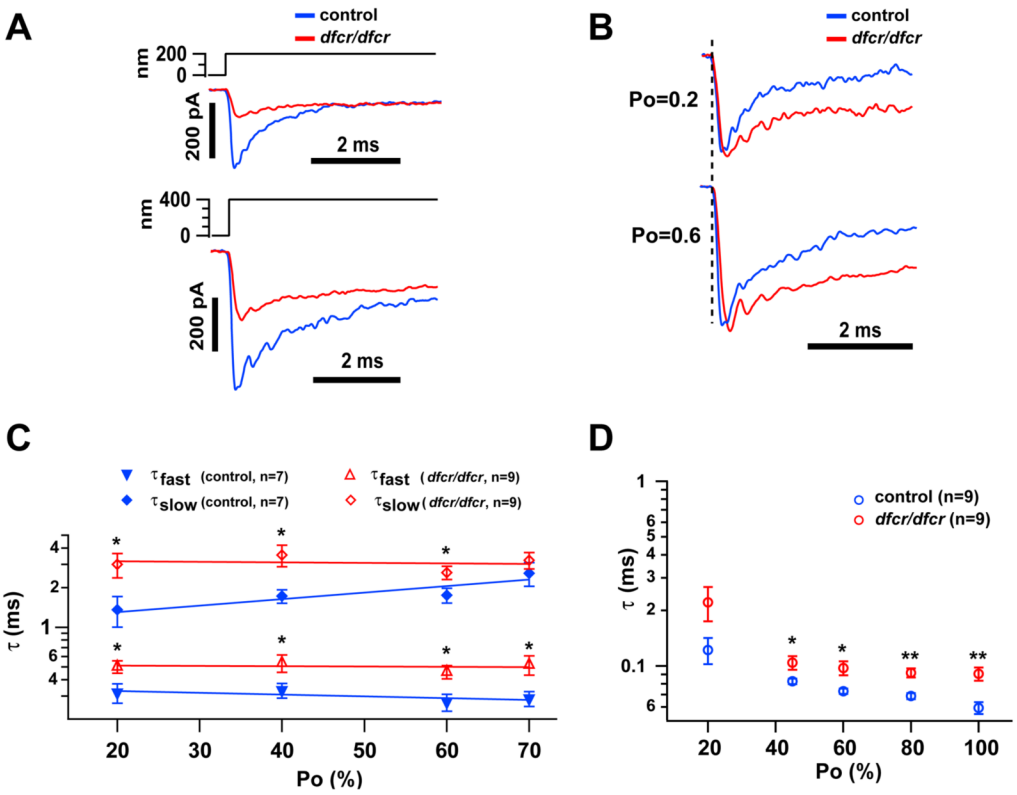

Fig. 6.

Analysis of adaptation in OHCs from *dfcr* mice. In all panels, data from hair cells of wild-type mice are represented in blue and from homozygous *dfcr* mice in red. (**A**) Average transduction currents in OHCs in response to a 200 nm and 400 nm deflection lasting for 5 ms. (**B**) Each averaged current trace from panel (A) was normalized to its peak current. (**C**) τ_{fast} and τ_{slow} were plotted against Po. τ_{fast} and τ_{slow} were significantly reduced in OHCs from *dfcr* mice. (**D**) The olot of activation time constants against Po revealed that channel activtion was slowed in *dfcr* mice. All data are shown as mean ± SEM. Student's two-tailed unpaired *t* test was used to determine statistical significance (*, $p<0.05$).

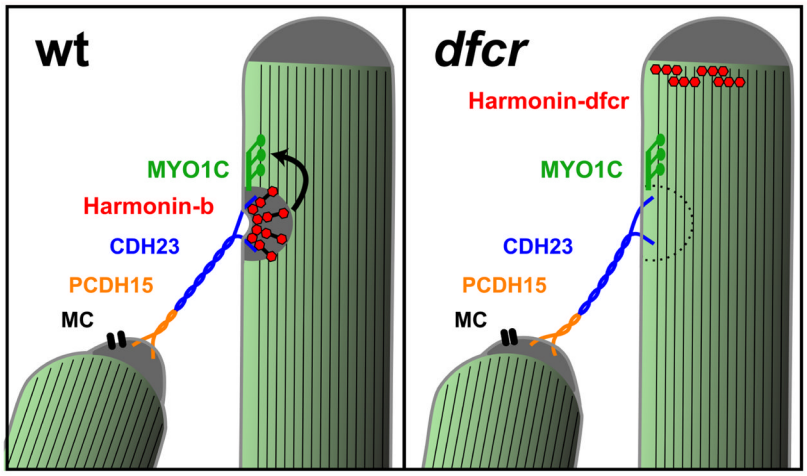

Fig. 7.

Model of harmonin function in mechanotransduction. The diagram highlights the asymmetric organization of the mechanotransduction machinery in hair cells, where the tip-link proteins CDH23 and PCDH15 are localized to the upper and lower tip-link part, respectively. MYO1C is positioned at the UTLD, the mechanotransduction channel (MC) at the LTLD, and harmonin is an integral part of the UTLD. According to the model, harmonin regulates MYO1C motor function but also bind to CDH23, F-actin and possibly the plasma membrane. Mislocalization of harmonin in *dfcr* mice affects MYO1C motor function and the interactions of the upper end of tip links with the membrane and cytoskeleton, affecting the force transmitted onto the mechanotransduction channel, here indicated by a slight bend in the tip-link filament.